PHYSICAL REVIEW A **97**, 053618 (2018)

Editors' Suggestion

Robustifying twist-and-turn entanglement with interaction-based readout

Safoura S. Mirkhalaf
QSTAR, Largo Enrico Fermi 2, 50125 Firenze, Italy

Samuel P. Nolan
School of Mathematics and Physics, The University of Queensland, Brisbane, Queensland 4072, Australia

Simon A. Haine*
Department of Physics and Astronomy, University of Sussex, Brighton, England BN1 9RH, United Kingdom

(Received 23 March 2018; published 25 May 2018)

The use of multiparticle entangled states has the potential to drastically increase the sensitivity of atom interferometers and atomic clocks. The twist-and-turn (TNT) Hamiltonian can create multiparticle entanglement much more rapidly than the ubiquitous one-axis twisting Hamiltonian in the same spin system. In this paper, we consider the effects of detection noise—a key limitation in current experiments—on the metrological usefulness of nonclassical states generated under TNT dynamics. We also consider a variety of interaction-based readouts to maximize their performance. Interestingly, the optimum interaction-based readout is not the obvious case of perfect time reversal.

DOI: 10.1103/PhysRevA.97.053618

I. INTRODUCTION

There is currently considerable interest in methods that can produce highly entangled states of atomic ensembles with the motivation of enhancing the sensitivity of atom interferometers and atomic clocks [1]. Without many-body entanglement, the phase sensitivity of such experiments is fundamentally shot-noise-limited (SNL) $\Delta\phi = 1/\sqrt{N}$ [2,3]. In recent years, experiments in atomic systems based on the one-axis twisting (OAT) spin squeezing scheme of Kitagawa and Ueda [4] (see also [5]) have demonstrated metrologically useful spin-squeezing [6,7], and sub-shot-noise phase detection [8–10]. However, typical experiments are limited to only moderate quantum enhancement due to constraints on the state preparation time imposed by dephasing [11,12] and multimode dynamics [13,14]. This leads to a degree of quantum enhancement that is considerably less than the theoretical optimum. Recently, a related method known as twist-and-turn (TNT) squeezing has been demonstrated [15–18]. The TNT Hamiltonian, which uses the same nonlinear interactions as OAT with an additional linear rotation, typically produces more quantum enhancement for the same interaction time. As TNT is based on the same interactions that lead to OAT squeezing, it can be implemented in the same experimental setups.

In practice, however, it is very difficult to fully exploit the nonclassical features of quantum states. This is mainly due to the fragility of quantum correlated states under inevitable sources of noise (e.g., phase or detection noise). One way to conquer these effects is to use *interaction-based readout* protocols [19–30] which make use of the appropriate supplementary unitary operations right before final measurement. These schemes can be summarized as follows. First there is a state preparation stage, where the quantum Fisher information (QFI, denoted F_Q) of the (typically unentangled) initial state $|\psi_0\rangle$ is increased via the unitary operator U_1. The QFI bounds the precision of an estimate via the quantum Cramér-Rao bound (QCRB), which states $\Delta\phi \geqslant 1/\sqrt{F_Q}$. The classical parameter to be estimated, ϕ, is then encoded onto the state via a measurement device (for example, a Mach-Zehnder interferometer) described by the unitary operator U_ϕ. The interaction-based readout is then implemented by applying another unitary operator $\hat{U}_2$ directly before the final measurement, such that the final state is

$$|\psi\rangle = U_2 U_\phi U_1 |\psi_0\rangle. \tag{1}$$

U_2 does not alter the QFI, but *can* affect the classical Fisher information (CFI, denoted F_c) when a measurement is made in a particular basis. Specifically, it has been shown that protocols which perfectly time reverse the initial unitary operator ($U_2 = U_1^\dagger$, which we refer to as an *echo*) followed by a measurement that projects onto the initial state saturates the QCRB [22], indicating the measurement is optimal. It has also been shown that using $U_2 = U_1^\dagger$ can improve robustness against detection noise [21,26]. However, in [26] it was shown that when a measurement that resolves the probability of *all* results in a particular basis is made, there are *many* choices of U_2 (including the trivial choice $U_2 = 1$) that saturate the QCRB. Furthermore, in many circumstances, there are choices for U_2 that provide greater robustness than $U_2 = U_1^\dagger$. In this paper we investigate how interaction-based readouts improve robustness specifically for the case where the state preparation (U_1) and interaction based readout (U_2) are based on the TNT interaction.

*simon.a.haine@gmail.com

II. INTERACTION-BASED READOUT PROTOCOL

Let us consider an ensemble of N two-level atoms which are prepared in initial state $|\psi_0\rangle$. The interaction-based readout protocol includes the following four steps.

(i) *State preparation:* This increases the QFI of the initial state via unitary evolution U_1 as $\rho = U_1|\psi_0\rangle\langle\psi_0|U_1^\dagger$. In particular, we use the TNT Hamiltonian for this purpose [defined in the next Section, Eq. (3)].

(ii) *Phase encoding:* An unknown phase is encoded into the state by performing linear unitary $U_\phi = e^{-i\phi\hat{S}_n}$ on the system such that $U_\phi^\dagger \rho U_\phi$. This process corresponds to making a rotation around an arbitrary spin direction $\vec{\boldsymbol{n}}$.

(iii) *Interaction-based readout:* A second entangling evolution U_2 is applied onto the state as $U_2 U_\phi \rho U_\phi^\dagger U_2^\dagger$. Echo protocols refer to the special case of perfect time reversal $U_2 = U_1^\dagger$. Under certain conditions, which we demonstrate below, U_2 allows measurements made in the appropriate basis to saturate the QCRB.

(iv) *Spin-resolving measurement:* A spin-resolving measurements projects on to some complete orthogonal basis $\{|m\rangle\}$. This is equivalent to estimating the full probability distribution $P_m(\phi) = \langle m|U_2 U_\phi \rho U_\phi^\dagger U_2^\dagger|m\rangle$.

Consequently, the phase ϕ can be estimated by examining the probabilities $P_m(\phi)$. Based on parameter estimation theory, the precision of the estimate is bounded by $\Delta\phi^2 = 1/F_c(\phi)$ where

$$F_c(\phi) = \sum_m \frac{1}{P_m(\phi)} \left(\frac{\partial P_m(\phi)}{\partial \phi}\right)^2 \tag{2}$$

is the CFI. For single-variate parameter estimation, it can be shown that a measurement basis yielding $F_c = F_Q$ is guaranteed to exist [31–33]. This measurement is optimal—the measurement saturates QCRB, which is the ultimate sensitivity limit imposed by ρ. As was shown in [26], the conditions that U_2 and the measurement basis $\{|m\rangle\}$ saturate the QCRB are (see Appendix A for a more detailed proof) the following.

(1) The initial state is the parity eigenstate in the measurement basis $\{|m\rangle\}$, i.e., $\hat{\Pi}\rho = (-1)^p\rho$ where $p = 0,1$ for $\hat{\Pi} = \sum_m (-1)^m |m\rangle\langle m|$.

(2) The generator $\hat{S}_n$ flips the parity, i.e., $\hat{\Pi}\hat{S}_n\hat{\Pi} = -\hat{S}_n$.

(3) The interaction-based readout U_2 conserves the parity with respect to the measurement basis, $[U_2, \hat{\Pi}] = 0$.

Thus, it is always possible to saturate the QCRB conditioned on suitable choices of measurement basis, readout, and phase generator. Conditions 1 and 2 can be used to determine the optimal measurement basis, which is typically easily accessible. Note that even for the trivial case of readout (i.e., $U_2 = 1$), so long as conditions 1 and 2 hold, the sensitivity saturates the QCRB [34]. Nevertheless, a nontrivial choice of U_2 (i.e., $U_2 \neq 1$) often increases the robustness against detection noise. In this spirit, we are allowed to pick the best readout strategy which satisfies the parity conservation requirement (the third condition).

In the following section, we consider the TNT Hamiltonian and demonstrate that the conditions for saturating the QCRB are satisfied.

III. TWIST-AND-TURN INTERFEROMETRY

We consider the TNT Hamiltonian [15–17]

$$H_{\rm TNT} = \hbar\chi\hat{S}_z^2 - \hbar J\hat{S}_x \tag{3}$$

such that $U_1 = \exp(-it_1 H_{\rm TNT}/\hbar)$, where the adjustable parameter t_1 is the state preparation time. Here, the collective spin operators obey the usual SU(2) commutation relations: $[\hat{S}_i, \hat{S}_j] = \epsilon_{ijk}\hat{S}_k$ where ϵ_{ijk} is the Levi-Civita symbol. Moreover, χ and J denote the magnitude of the spin-spin interaction and the rate of rotation about the $\hat{S}_x$ axis, respectively. One can alter the macroscopic properties of the system by adjusting the parameter $\Lambda = N\chi/J$ [36,37], where N is the total number of particles. Specifically, it has been shown that $\Lambda = 2$, corresponding to maximal criticality of the unstable fixed point in mean-field approximation, provides the maximum rate of entanglement generation [15,18]. In the limit of $\chi \gg J$ the TNT Hamiltonian reduces to the well-known one-axis-twisting form $H_{\rm OAT} = \hbar\chi\hat{S}_z^2$.

The TNT Hamiltonian can accelerate the rate of entanglement generation compared to the OAT Hamiltonian for the same χt_1 [17]. This is the direct consequence of interplay between twist ($\propto \hat{S}_z^2$) and turn ($\propto \hat{S}_x$) terms of the Hamiltonian. The generation of spin squeezing under TNT dynamics has been investigated theoretically [15–18,38] and realized experimentally in atomic Bose-Einstein condensates [16,17] and cold atomic ensembles [39].

Figure 1 shows the time evolution of the SU(2) Husimi Q function [35,40], and the QFI under TNT dynamics. The QFI is defined as $F_Q = 4\Delta S_n^2$, where $\hat{S}_n$ is the collective spin operator pointing in the direction that maximizes the QFI [41]. However, the QFI is silent on what measurement choice saturates the QCRB. If the ϕ estimate is obtained from the mean spin component $\langle\hat{S}_{n'}\rangle$, the error propagation formula gives $\Delta\phi^2 = \Delta S_{n'}^2/\partial_\phi\langle\hat{S}_{n'}\rangle = \xi^2/N$, where $\xi^2 = N\Delta S_{n'}^2/\langle\hat{S}_\parallel\rangle^2$ is the spin-squeezing parameter normal to mean spin direction $\hat{S}_\parallel$ [42]. For small values of χt_1, this method of estimation is very close to the QCRB, but breaks down when the state becomes non-Gaussian. Non-Gaussian states with $F_Q > N$ are called entangled non-Gaussian states (ENGS), and an analysis of their CFI reveals their metrological gain can exceed that of spin-squeezed states [3,16,21,22,43].

We now consider the requirements for performing a measurement that saturates the QCRB with a state generated via TNT dynamics. Assuming the initial state is an eigenstate of $\hat{S}_x$, then $H_{\rm TNT}$ couples only to $\hat{S}_x$ eigenstates of the same parity. That is, U_1 conserves parity with respect to the $\hat{S}_x$ eigenbasis $\{|m\rangle_x\}$ [44,45]. Subsequently, we align the interferometer along the optimal F_Q direction such that $U_\phi = \exp(i\hat{S}_n\phi)$. It has been shown that this operator is in the y-z plane, i.e., $\hat{S}_n = \alpha\hat{S}_y + \beta\hat{S}_z$ normal to the mean spin direction $\hat{S}_x$ [18]. Since the generator of the interferometer $\hat{S}_n$ flips the parity (i.e., $\hat{\Pi}\hat{S}_n\hat{\Pi} = -\hat{S}_n$, for $\hat{\Pi} = \sum_m |m\rangle_x\langle m|_x$), we see that a measurement that projects into the $\hat{S}_x$ eigenbasis will saturate the QCRB. This is applicable to all readouts that conserve parity with respect to $\hat{S}_x$ (see Appendix B for details).

In realistic situations, however, there is detection noise which limits the estimation sensitivity. Both spin-squeezed states and ENGS are more sensitive to detection noise than unentangled states of the same size, and ENGS typically

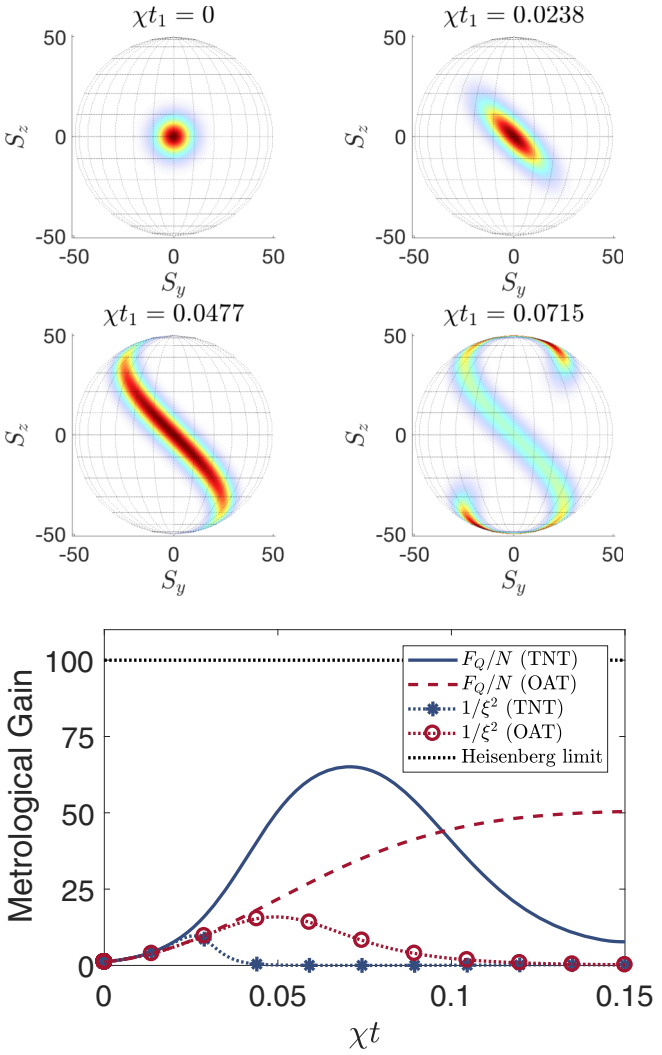

FIG. 1. Upper panel: Husimi Q function for the state $|\psi\rangle = \exp(-itH_{\rm TNT}/\hbar)|\psi_0\rangle$ under TNT with $\Lambda = 2$ and $N = 100$, where $|\psi_0\rangle$ is chosen as the eigenstate of $\hat{S}_x$ with minimum eigenvalue. From left to right: $\chi t = 0$, 0.0238, 0.0477, and 0.0715. The final frame is the time at which the QFI is maximum. Bloch-sphere plots display the SU(2) Husimi Q function $Q/Q_{\rm max}$, which is defined $Q(\theta,\varphi) = \langle\theta,\varphi|\rho|\theta,\varphi\rangle$, where $|\theta,\varphi\rangle = e^{i\varphi\hat{S}_z}e^{i\theta\hat{S}_y}|S_z = N/2\rangle$ represents the spin coherent state along θ and φ directions corresponding to rotating the maximal $\hat{S}_z$ eigenstate around azimuthal and polar angles $\{\theta,\varphi\}$ [35]. Lower panel: Metrological gain F_Q/N as a function of χt for TNT (blue solid) and OAT (red dashed). We have also included the gain based on spin-squeezing parameter for TNT (blue solid pentagram) and OAT (red solid circles). The Heisenberg limit ($\Delta\phi = 1/N$) is indicated by the black dotted line. The initial state is chosen to be the minimal eigenstate of S_x.

demand detection noise at the single-atom level [1,25,26], which restricts them to small numbers as the requisite counting efficiency rapidly becomes impossible. For this reason, detection noise is a key limitation in current experiments [1].

The effect of detection noise is to introduce additional, classical noise to the measurement process. For example, a detector that measures the spin projection along $\hat{S}_x$ should always read $S_x = N/2$ for a maximal $\hat{S}_x$ eigenstate. However, if there is noise introduced, there is a finite chance that the

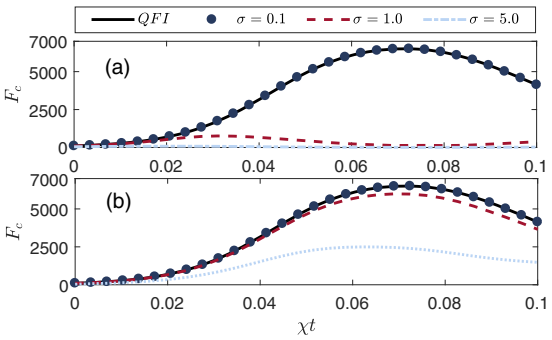

FIG. 2. Time evolution of the QFI (solid black) and CFI for various detection noises $\sigma = 0.1$ (dotted blue), 1.0 (dashed red), and 5.0 (dotted-dashed light turquoise) for the final state $U_2U_\phi U_1|\psi_0\rangle$, for (a) $U_2 = 1$ and (b) $U_2 = U_1^\dagger$. In all cases the initial state is chosen to be the minimal eigenstate of S_x and we have fixed $\phi = 10^{-4}$.

detector will read $S_x = m \neq N/2$. To model detection noise we follow [1,26,46] and take the convolution of the probability distribution with a Gaussian distribution with detection noise σ:

$$\tilde{P}_m(\phi) = \sum_{m'} C_{m'}(\sigma)\exp[-(m-m')^2/2\sigma^2]P_{m'}(\phi). \quad (4)$$

Imposing $\sum_m \tilde{P}_m(\phi) = 1$ one obtains the appropriate normalization factor:

$$C_{m'}(\sigma) = \left(\sum_m \exp[-(m-m')^2/2\sigma^2]\right)^{-1}. \quad (5)$$

We note that this is equivalent to introducing the positive-operator-valued measurement (POVM) [47]

$$\{\hat{M}_m\} = \{|m\rangle\langle m|\} = \sum_{m'} C_{m'}(\sigma)e^{-(m-m')^2/2\sigma^2}|m'\rangle\langle m'| \quad (6)$$

such that the probability distribution of making measurements on the noisy POVMs is given by $\tilde{P}_m(\phi) = {\rm Tr}(\hat{M}_m U_2 U_\phi \rho U_\phi^\dagger U_2^\dagger)$. Note that in the limit of negligible detection noise ($\sigma \to 0$) the POVMs approach the orthogonal basis (Sec. II). In Fig. 2(a) we show the CFI calculated from this convolved probability distribution $\tilde{P}_m$ for the state $U_\phi U_1|\psi_0\rangle$, for different values of σ. For $\sigma \lesssim 0.1$, our measurement saturates the QCRB. However, for moderate values of χt_1, a small increase in detection noise significantly degrades the sensitivity. Fortunately, by adding an interaction-based readout such that the final state is $U_2U_\phi U_1|\psi_0\rangle$, with $U_2 = U_1^\dagger$, the sensitivity is much more robust to the presence of noise [Fig. 2(b)].

We can understand why the interaction-based echo makes the system so much more robust by looking at the Q function and the probability distributions. Figure 3 shows the Q functions and S_x probability distribution for states with $\phi = 0$ and a small phase shift $\delta\phi$, for the case with ($U_2 = U_1^\dagger$) and without ($U_2 = 1$) an interaction-based readout. In the absence of detection noise, the fidelity between the state with $\phi = 0$ and $\delta\phi$ is identical with and without the interaction-based readout. Similarly, the Hellinger distance between the

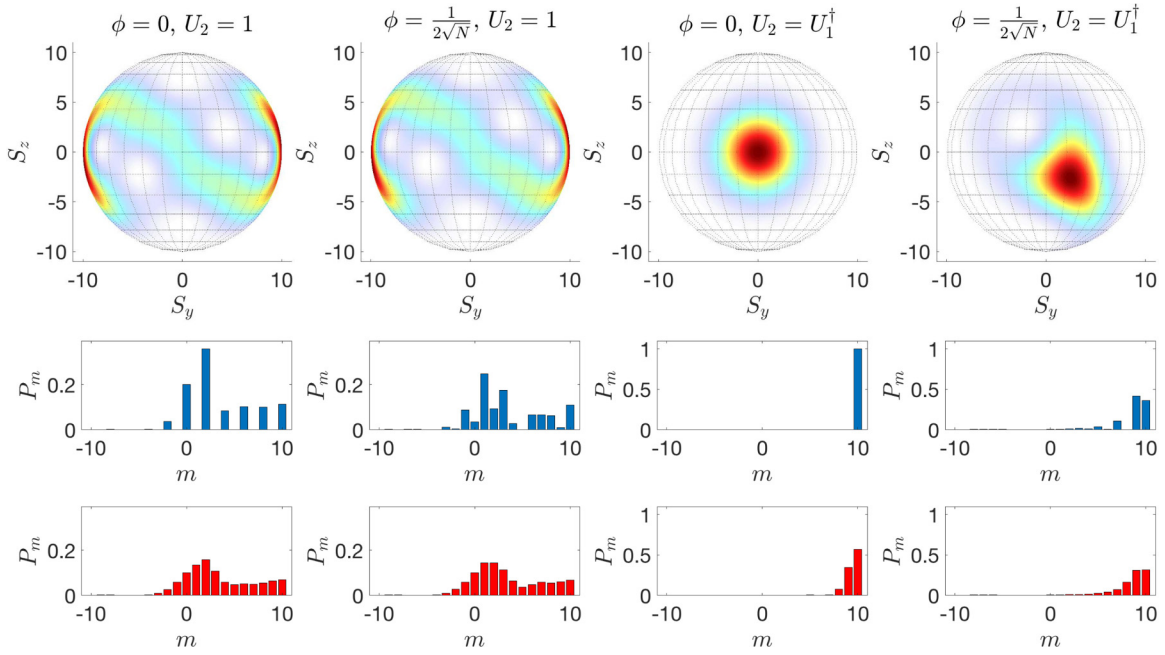

FIG. 3. Top row: Husimi Q function for the final state for (from left to right) $\phi = 0, U_2 = 1; \phi = \frac{1}{2\sqrt{N}}, U_2 = 1; \phi = 0, U_2 = U_1^\dagger; \phi = \frac{1}{2\sqrt{N}}$, $U_2 = U_1^\dagger$. Middle row (blue histograms): The corresponding probabilities P_m for measurements in the S_x eigenbasis for these same states. Bottom row (red histograms): Probabilities in the S_x eigenbasis convolved with detection noise with $\sigma = 1$. Parameters: $N = 20$, $\Lambda = 2$, and $\chi t = 0.275$, which maximizes F_Q. Note that for reasons of visual clarity, we have rotated the state around the S_x axis such that $S_n = S_y$.

distributions is also identical. The Hellinger distance defines a statistical distance between $P_m(\phi_1)$ and $P_m(\phi_2)$, defined as $d_H^2(\phi_1,\phi_2) = 1 - \sum_m \sqrt{P_m(\phi_1)P_m(\phi_2)}$. Adding detection noise, it becomes difficult to distinguish the distributions when $U_2 = 1$. Compare this to $U_2 = U_1^\dagger$, and the two distributions are more easily distinguished. Quantitatively, without the interaction-based readout, the Hellinger distance is $d_H^2 = 0.01$, but when we include the readout it is significantly larger: $d_H^2 = 0.17$ (compared to $d_H^2 = 0.40$ in both cases when no noise is included). However, there is no guarantee that $U_2 = U_1^\dagger$ is the best choice of interaction-based readout. In the next section, we examine several possibilities to determine what is the best choice for maximizing robustness in TNT squeezing.

IV. ROBUSTIFYING ENTANGLEMENT AGAINST DETECTION NOISE

We now examine the robustness to detection noise, for different choices of U_2, all satisfying the conditions for optimality. In particular, we chose the trivial case of no interaction-based readout ($U_2 = 1$), and the simple time-reversal readout [$U_2 = U_1^\dagger(t_2)$]. The latter choice includes asymmetric echo where $t_2 \neq t_1$, which implies $U_2 \neq U_1^\dagger$. In this case, we have increased the interaction time for the readout compared to the state preparation step. Moreover, we also include $U_2 = U_1$, which may be applicable in the case when it is not easy to reverse the sign of the interaction constant χ, such as when one is working with bright solitons [48], or enhanced nonlinear interactions due to state-dependent potentials [9].

Figure 4 shows F_c as a function of detection noise for different choices of U_2 when $\chi t_1 = 0.027$ (when the metrological gain using the spin-squeezing parameter is maximum) and 0.072 (when the QFI is maximum). For the case of weak entanglement ($\chi t_1 = 0.027$), we see that the trivial case ($U_2 = 1$) is degraded to below shot-noise levels for noise of approximately $\sigma \approx 4.40$. However, by adding the "echo" unitary ($U_2 = U_1^\dagger$), sub-shot-noise sensitivities are retained up to $\sigma \approx 16.45$. Interestingly the choice $U_2 \neq U_1^\dagger$ provides greater robustness again, with sub-shot-noise sensitivities with up to $\sigma = 39.17$, which is significantly greater than $\sqrt{N}$. For this value of χt_1, $U_2 = U_1$ provides no advantage compared to the trivial case. However, for the case of maximum QFI ($\chi t = 0.072$), this choice does provide some additional robustness compared to the trivial case. The asymmetric echo provides the greatest robustness of the schemes considered, and therefore may be useful when there is unavoidably large detection noise. To obtain F_c, we have numerically optimized the measurement basis in the planes normal to $\hat{S}_x$ and $\hat{S}_n$ [49]. Based on our numerical calculations, it seems that by increasing the detection noise, the optimal measurement basis moves into the normal plane to S_x.

We now more closely examine the effect of an asymmetric echo on the TNT scheme. In Fig. 5, we have changed the time duration of the echo t_2/t_1 for fixed detection noises $\sigma = 0.1,5.0$ when the TNT Hamiltonian produces the maximum value of spin squeezing ($t_1 = 0.027$) or maximum value of quantum Fisher information ($t_1 = 0.072$), respectively. For small values of detection noise $\sigma = 0.1$, U_2 does not affect the classical Fisher information. In this case, as mentioned before, F_c saturates the QCRB. In contrast, for more noise ($\sigma = 5.0$) we see that in the Gaussian regime ($t_1 = 0.027$), by increasing the duration of the echo (t_2/t_1), the sensitivity becomes more robust against detection noise and eventually approaches the QCRB value for large enough t_2. Compare this

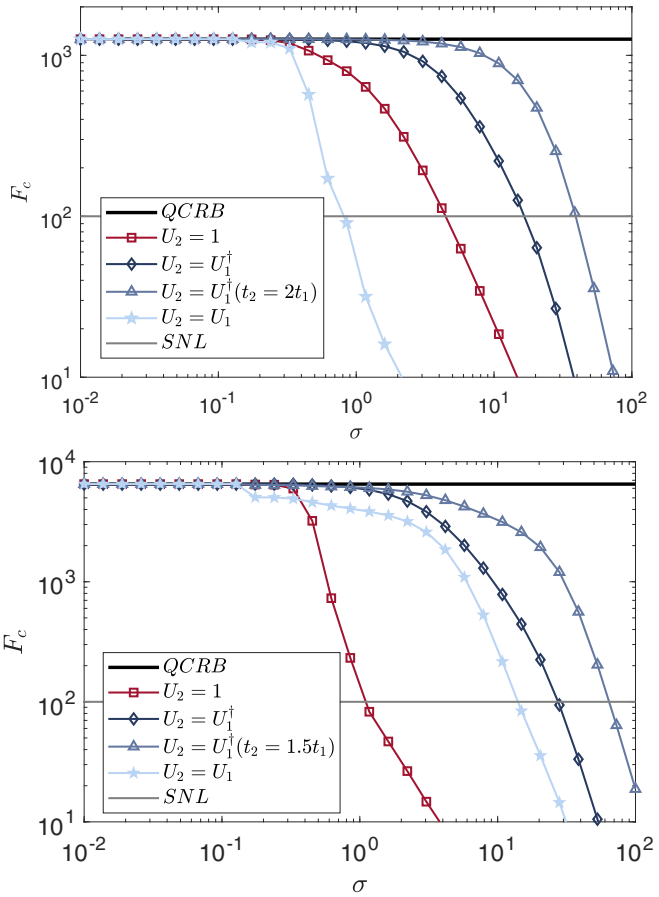

FIG. 4. Decay of classical Fisher information for a many-body entangled state produced by the TNT Hamiltonian in presence of detection noise σ for $N = 100$, $\Lambda = 2$, and $\chi t_1 = 0.027$ (upper panel) and $\chi t_1 = 0.072$ (lower panel). We have considered the trivial protocol $U_2 = 1$ (red squares), an echo $U_2 = U_1^\dagger$ (dark blue diamonds), an asymmetric echo $U_2 \neq U_1^\dagger$ (light blue triangles), and a pseudoecho $U_2 = U_1$ (light turquoise pentagrams). We have also considered QCRB and SNL as thick black and thin gray lines, respectively. Here, $\phi = 10^{-4}$.

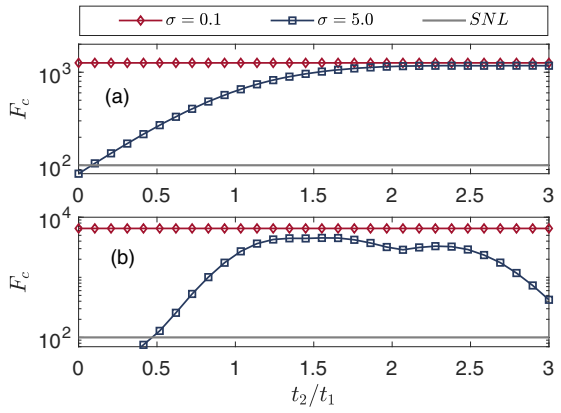

FIG. 5. The Fisher information produced by TNT vs time duration of echo t_2/t_1 for $U_2 = U_1^\dagger(t_2)$ in presence of detection noise $\sigma = 0.1$ (red diamonds) and 5.0 (blue squares) when (a) spin squeezing is maximum $t_1 = 0.027$ and (b) the QFI is maximum $t_1 = 0.072$. For both cases, when there is negligible detection noise, the CFI corresponds to QCRB as expected. The SNL is the gray line.

to the non-Gaussian regime ($t_1 = 0.072$), where there is a clear optimum readout time of roughly $t_2/t_1 \approx 1.5$. Recently, similar behavior has been reported in the two-axis-counter-twisted interaction-based readout scheme [28].

In a realistic spin-squeezing setup, the duration of the experiment may be limited by the particle losses as well as dephasing [11,12] and multimode dynamics [13,14]. Therefore, it is important to consider the optimal portion of time for entangling (U_1) and reentangling (U_2) sequences, as there is a tradeoff between the desire to maximize the QFI via the state preparation operation $U_1(t_1)$, and robustifying against detection noise via the interaction-based readout operation $U_2(t_2)$, while keeping the total time fixed $T = t_1 + t_2$. In Fig. 6 we have given the optimized Fisher information versus entangling unitary time for total experimental duration $T = 0.1$ with $N = 100$ and $\Lambda = 2$ and time-reversal echo case $U_2 = U_1^\dagger$. When the detection noise is small ($\sigma = 0.1$), there is little benefit in increasing t_2 and the optimum strategy is to choose $U_2 = 1$. However, this is certainly not true for large detection noise, as devoting more time to the entangling operation compromises the interaction-based readout. Therefore, to maximize the CFI there is a balance to be found between twisting the initial state for longer time (increasing t_1) and robustifying the state (increasing t_2). For larger values of detection noise ($\sigma = 1.0$, 5.0) we see that the optimal strategy is close to an echo ($t_1 \approx T/2 = 0.050$). The reason is that when we devote less than half of the time to the TNT entangling operation, there is always a possibility to perform an echo with $t_2/t_1 \geqslant 1$. Thus, the decrease in F_c as a result of reducing the first TNT unitary is compensated for by increased robustness provided by the second unitary. For instance, Fig. 5(a) gives the typical behavior of the asymmetric echo within this region, which approaches the QCRB as t_2/t_1 increases beyond 1. On the other

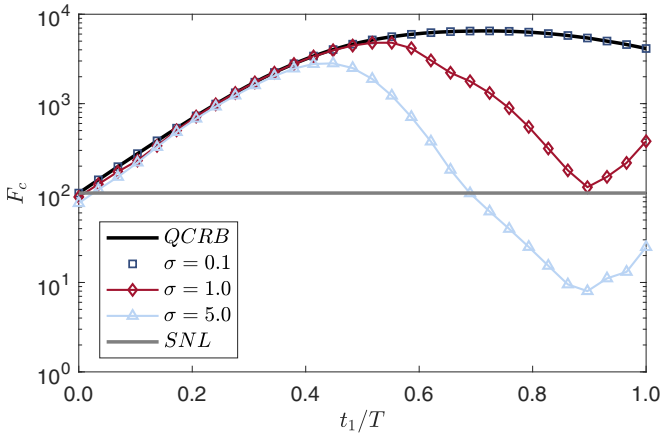

FIG. 6. Classical Fisher information vs entangling duration t_1, with fixed total experimental time $\chi T = \chi(t_1 + t_2) = 0.1$. The TNT entanglement and reentangling operation $[U_2 = U_1^\dagger(t_2)]$ are applied for durations t_1 and $t_2 = T - t_1$, respectively, such that $|\psi_\phi\rangle = U_1^\dagger(t_2)U_\phi U_1(t_1)|\psi_0\rangle$. Here, $N = 100$ and $\Lambda = 2$ and we have considered $\sigma = 0.1$ (dark blue squares), 1.0 (red diamonds), and $\sigma = 5.0$ (light turquoise triangles). The QCRB and SNL are given with solid thick black and thin gray lines.

hand, by increasing the portion of the entangling duration more than $T/2$, the echo time ratio t_2/t_1 decreases below unity, and is far more susceptible to detection noise.

V. CONCLUSION

Many-body entangled states are crucial resources for quantum-enhanced metrology. Current experiments are working to devise schemes that are able to rapidly manufacture these states in large atomic ensembles, but detection noise is currently a key limitation [1]. The TNT interaction is capable of generating entanglement faster than the conventional one-axis-twisting interaction. TNT is capable of rapidly producing both spin-squeezed states and ENGS. In this paper we explore the use of interaction-based readout protocols to provide rapid quantum-enhanced metrology based on twist-and-turn dynamics, which is also robust to detection noise and optimally utilizes the state's entanglement. This is done with a spin-resolving measurement in the optimal basis, which we provide criteria for determining. In this regard, we have confirmed the usefulness of standard symmetric echo protocols in boosting the measurement performance against noise. However, our results imply that for weakly entangled initial states using an asymmetric echo provides better robustness than the symmetric case. Finally, we have considered TNT echo protocols in a realistic situation where there is a limitation on the total time allowed for both the initial interaction and the readout. We have shown that the best outcomes require balance between entangling and reentangling time durations. When detection noise is small, any readout is suboptimal. In presence of considerable noise, the optimal strategy is close to an echo, but the precise time tradeoff depends on the magnitude of detection noise present in the system.

ACKNOWLEDGMENTS

The authors acknowledge useful discussions with Augusto Smerzi, Luca Pezze, and Manuel Gessner. Numerical simulations were performed on the University of Queensland School of Mathematics and Physics computing cluster "Dogmatix," with thanks to I. Mortimer for computing support. S.P.N. acknowledges support provided by an Australian Postgraduate Award. S.A.H. has received funding from the European Union's Horizon 2020 research and innovation programme under the Marie Sklodowska-Curie Grant Agreement No. 704672.

APPENDIX A: THE CONDITIONS OF QCRB SATURATION

Here, we present our conditions for saturation of QCRB (Sec. II) when applying spin-resolving measurement [26].

To begin, let us ignore the reentangling readout operator, and consider only $U_2 = 1$. After the state preparation and phase encoding steps, the probability of estimating the small, unknown phase ϕ is given by $P_m(\phi) = \langle m|U_\phi \rho U_\phi^\dagger|m\rangle$ with $U_\phi = e^{(-iS_n\phi)}$. Our phase estimation is limited by the CFI. For small values of ϕ the CFI can be approximated as the leading term in the expansion of the Hellinger statistical distance in the space of probability distributions [16]:

$$d_H^2(0,\phi) = 1 - \sum_m \sqrt{P_m(0)P_m(\phi)} = F_c(0)\phi^2/8 + O(\phi^3). \tag{A1}$$

For small ϕ, Taylor expanding the probability amplitude gives

$$P_m(\phi) = P_m(0) + \left.\frac{\partial P_m(\phi)}{\partial\phi}\right|_{\phi=0}\phi + \left.\frac{\partial^2 P_m(\phi)}{\partial\phi^2}\right|_{\phi=0}\frac{\phi^2}{2} + \mathcal{O}(\phi^3). \tag{A2}$$

We have

$$\begin{aligned} P_m(\phi) &= \langle m|U_\phi^\dagger \rho U_\phi|m\rangle, \\ \frac{\partial P_m(\phi)}{\partial\phi} &= i\langle m|\hat{S}_n U_\phi \rho U_\phi^\dagger|m\rangle + \text{c.c.}, \\ \frac{\partial^2 P_m(\phi)}{\partial\phi^2} &= \langle m|\hat{S}_n U_\phi \rho U_\phi^\dagger \hat{S}_n|m\rangle \\ &\quad - \langle m|\hat{S}_n^2 U_\phi \rho U_\phi^\dagger|m\rangle + \text{c.c.}, \end{aligned} \tag{A3}$$

which leads to

$$\begin{aligned} P_m(0) &= \langle m|\rho|m\rangle, \\ \left.\frac{\partial P_m(\phi)}{\partial\phi}\right|_{\phi=0} &= i\langle m|\hat{S}_n\rho|m\rangle + \text{c.c.}, \\ \left.\frac{\partial^2 P_m(\phi)}{\partial\phi^2}\right|_{\phi=0} &= \langle m|\hat{S}_n\rho\hat{S}_n|m\rangle \\ &\quad - \langle m|\hat{S}_n^2\rho|m\rangle + \text{c.c.} \end{aligned} \tag{A4}$$

Now, suppose that the density operator is an eigenstate of the parity operator $\hat{\Pi} = \sum_m (-1)^m |m\rangle\langle m|$ such that $\hat{\Pi}\rho = (-1)^p\rho$ for $p = 0,1$. Also, let $\hat{\Pi}\hat{S}_n\hat{\Pi} = -\hat{S}_n$ (Sec. II). Under these two conditions,

$$\begin{aligned} &\langle m|\rho|m\rangle = (-1)^{m+p}\langle m|\rho|m\rangle, \quad \langle m|\rho\hat{S}_n|m\rangle = 0, \\ &\langle m|S_n\rho\hat{S}_n|m\rangle = (-1)^{m+p+1}\langle m|\hat{S}_n\rho\hat{S}_n|m\rangle, \end{aligned} \tag{A5}$$

which also yields

$$P_m(0)\langle m|\hat{S}_n\rho\hat{S}_n|m\rangle = 0, \tag{A6}$$

as $P_m(0) = 0$ if $m + p$ is odd, and $\langle m|\hat{S}_n\rho\hat{S}_n|m\rangle = 0$ if $m + p$ is even. After using (A2) and (A6) in (A1) followed by a binomial expansion of square root for small ϕ, we obtain

$$d_H^2(\phi) = \sum_m \langle m|\hat{S}_n^2\rho|m\rangle/2 \tag{A7}$$

up to third order in ϕ. Finally, as $\langle\hat{S}_n\rangle = 0$ [Eq. (A5)], up to third order in ϕ the Fisher information is

$$F_c(0) = 4\sum_m \langle m|\hat{S}_n^2\rho|m\rangle = 4\Delta\hat{S}_n^2 = F_Q \tag{A8}$$

where ΔS_n^2 is the variance of generator. The last equality appears since $F_c \leqslant F_Q \leqslant \Delta S_n^2$. Thus, the first two parity conditions (Sec. II) ensure the saturation of the QCRB. There is no need to use the reentangling step to obtain this result. However, in order to robustify the scheme against noise, we include the readout operator U_2 after phase encoding, which gives $P_m(\phi) = \langle m|U_2^\dagger U_\phi^\dagger \rho U_\phi U_2|m\rangle$. This probability distribution has equivalent CFI when compared to the distribution

$P'_m = \langle m|U_\phi^\dagger \rho U_\phi|m\rangle$ if $[U_2, \hat{\Pi}] = 0$, i.e., the readout operator has the same parity as measurement basis $|m\rangle$ (condition 3 given in Sec. II).

APPENDIX B: FULFILLMENT OF PARITY CONDITIONS FOR THE TNT SCENARIO

The TNT Hamiltonian conserves parity, $[H_{\rm TNT}, \hat{\Pi}_x] = 0$ [44,45]. Consequently by taking the initial state as the $\hat{S}_x$ eigenstate, the first parity condition of Sec. II is satisfied. Moreover, the parity symmetry leads to $\hat{\Pi}_x(\hat{S}_x, \hat{S}_y, \hat{S}_z)\hat{\Pi}_x = (\hat{S}_x, -\hat{S}_y, -\hat{S}_z)$. Considering the fact that optimal QFI is in the y-z plane [16,18] $\hat{S}_n = \alpha\hat{S}_y + \beta\hat{S}_z$, one obtains $\hat{\Pi}_x\hat{S}_n\hat{\Pi}_x = -\hat{S}_n$ which demonstrates the second condition. To demonstrate the third condition, we again note that the reentangling unitary conserves parity in the $\hat{S}_x$ eigenbasis. Of course, asymmetry in the entangling and reentangling operations does not affect this result.

[1] L. Pezze, A. Smerzi, M. K. Oberthaler, R. Schmied, and P. Treutlein, Quantum metrology with nonclassical states of atomic ensembles, arXiv:1609.01609 (2016).

[2] V. Giovannetti, S. Lloyd, and L. Maccone, Quantum Metrology, Phys. Rev. Lett. **96**, 010401 (2006).

[3] L. Pezzé and A. Smerzi, Entanglement, Nonlinear Dynamics, and the Heisenberg Limit, Phys. Rev. Lett. **102**, 100401 (2009).

[4] M. Kitagawa and M. Ueda, Squeezed spin states, Phys. Rev. A **47**, 5138 (1993).

[5] K. Mølmer and A. Sørensen, Multiparticle Entanglement of Hot Trapped Ions, Phys. Rev. Lett. **82**, 1835 (1999).

[6] J. Esteve, C. Gross, A. Weller, S. Giovanazzi, and M. K. Oberthaler, Squeezing and entanglement in a Bose-Einstein condensate, Nature (London) **455**, 1216 (2008).

[7] I. D. Leroux, M. H. Schleier-Smith, and V. Vuletić, Implementation of Cavity Squeezing of a Collective Atomic Spin, Phys. Rev. Lett. **104**, 073602 (2010).

[8] C. Gross, T. Zibold, E. Nicklas, J. Estève, and M. K. Oberthaler, Nonlinear atom interferometer surpasses classical precision limit, Nature (London) **464**, 1165 (2010).

[9] M. F. Riedel, P. Böhi, Y. Li, T. W. Hänsch, A. Sinatra, and P. Treutlein, Atom-chip-based generation of entanglement for quantum metrology, Nature (London) **464**, 1170 (2010).

[10] W. Muessel, H. Strobel, D. Linnemann, D. B. Hume, and M. K. Oberthaler, Scalable Spin Squeezing for Quantum-Enhanced Magnetometry with Bose-Einstein Condensates, Phys. Rev. Lett. **113**, 103004 (2014).

[11] Yun Li, Y. Castin, and A. Sinatra, Optimum Spin Squeezing in Bose-Einstein Condensates with Particle Losses, Phys. Rev. Lett. **100**, 210401 (2008).

[12] Yun Li, P. Treutlein, J. Reichel, and A. Sinatra, Spin squeezing in a bimodal condensate: Spatial dynamics and particle losses, Eur. Phys. J. B **68**, 365 (2009).

[13] S. A. Haine and M. T. Johnsson, Dynamic scheme for generating number squeezing in Bose-Einstein condensates through nonlinear interactions, Phys. Rev. A **80**, 023611 (2009).

[14] S. A. Haine, J. Lau, R. P. Anderson, and M. T. Johnsson, Self-induced spatial dynamics to enhance spin squeezing via one-axis twisting in a two-component Bose-Einstein condensate, Phys. Rev. A **90**, 023613 (2014).

[15] A. Micheli, D. Jaksch, J. I. Cirac, and P. Zoller, Many-particle entanglement in two-component Bose-Einstein condensates, Phys. Rev. A **67**, 013607 (2003).

[16] H. Strobel, W. Muessel, D. Linnemann, T. Zibold, D. B. Hume, L. Pezzè, A. Smerzi, and M. K. Oberthaler, Fisher information and entanglement of non-Gaussian spin states, Science **345**, 424 (2014).

[17] W. Muessel, H. Strobel, D. Linnemann, T. Zibold, B. Juliá-Díaz, and M. K. Oberthaler, Twist-and-turn spin squeezing in Bose-Einstein condensates, Phys. Rev. A **92**, 023603 (2015).

[18] G. Sorelli, L. Pezze, and A. Smerzi, Fast generation of entanglement in bosonic Josephson junctions, arXiv:1511.01835 (2015).

[19] A. M. Marino, N. V. Corzo Trejo, and P. D. Lett, Effect of losses on the performance of an SU(1,1) interferometer, Phys. Rev. A **86**, 023844 (2012).

[20] O. Hosten, R. Krishnakumar, N. J. Engelsen, and M. A. Kasevich, Quantum phase magnification, Science **352**, 1552 (2016).

[21] E. Davis, G. Bentsen, and M. Schleier-Smith, Approaching the Heisenberg Limit without Single-Particle Detection, Phys. Rev. Lett. **116**, 053601 (2016).

[22] T. Macrì, A. Smerzi, and L. Pezzè, Loschmidt echo for quantum metrology, Phys. Rev. A **94**, 010102 (2016).

[23] F. Fröwis, P. Sekatski, and W. Dür, Detecting Large Quantum Fisher Information with Finite Measurement Precision, Phys. Rev. Lett. **116**, 090801 (2016).

[24] S. S. Szigeti, R. J. Lewis-Swan, and S. A. Haine, Pumped-Up SU(1,1) Interferometry, Phys. Rev. Lett. **118**, 150401 (2017).

[25] E. Davis, G. Bentsen, T. Li, and M. Schleier-Smith, Advantages of interaction-based readout for quantum sensing, in *Proceedings of the Advances in Photonics of Quantum Computing, Memory, and Communication X*, Vol. 10118 (SPIE, Washington, 2017), p. 101180Z.

[26] S. P. Nolan, S. S. Szigeti, and S. A. Haine, Optimal and Robust Quantum Metrology using Interaction-Based Readouts, Phys. Rev. Lett. **119**, 193601 (2017).

[27] J. Huang, M. Zhuang, and C. Lee, Non-Gaussian precision metrology via driving through quantum phase transitions, Phys. Rev. A **97**, 032116 (2018).

[28] F. Anders, L. Pezzè, A. Smerzi, and C. Klempt, Phase magnification by two-axis countertwisting for detection-noise robust interferometry, Phys. Rev. A **97**, 043813 (2018).

[29] R. Fang, R. Sarkar, and S. M. Shahriar, Enhancing sensitivity of an atom interferometer to the Heisenberg limit using increased quantum noise, arXiv:1707.08260 (2017).

[30] A. J. Hayes, S. Dooley, W. J. Munro, K. Nemoto, and J. Dunningham, Making the most of time in quantum metrology: Concurrent state preparation and sensing, arXiv:1801.03452 (2018).

[31] S. L. Braunstein and C. M. Caves, Statistical Distance and the Geometry of Quantum States, Phys. Rev. Lett. **72**, 3439 (1994).

[32] Géza Tóth and I. Apellaniz, Quantum metrology from a quantum information science perspective, J. Phys. A **47**, 424006 (2014).

[33] R. Demkowicz-Dobrzański, M. Jarzyna, and J. Kołodyński, Quantum limits in optical interferometry, Prog. Opt. **60**, 345 (2015).

[34] Also, note that using U_2 does not change the QFI. This can be easily verified when using the equation $F_Q = 4[\langle\partial_\phi\psi|\partial_\phi\psi\rangle - |\langle\psi|\partial_\phi\psi\rangle|^2]$ for $|\psi\rangle = U_2U_\phi U_1|\psi_0\rangle$ where $\partial_\phi = \partial/\partial\phi$.

[35] F. T. Arecchi, Eric Courtens, Robert Gilmore, and Harry Thomas, Atomic coherent states in quantum optics, Phys. Rev. A **6**, 2211 (1972).

[36] A. Smerzi, S. Fantoni, S. Giovanazzi, and S. R. Shenoy, Quantum Coherent Atomic Tunneling between Two Trapped Bose-Einstein Condensates, Phys. Rev. Lett. **79**, 4950 (1997).

[37] G. J. Milburn, J. Corney, E. M. Wright, and D. F. Walls, Quantum dynamics of an atomic Bose-Einstein condensate in a double-well potential, Phys. Rev. A **55**, 4318 (1997).

[38] Guang-Ri Jin and Sang Wook Kim, Spin squeezing and maximal-squeezing time, Phys. Rev. A **76**, 043621 (2007).

[39] S. Chaudhury, S. Merkel, T. Herr, A. Silberfarb, I. H. Deutsch, and P. S. Jessen, Quantum Control of the Hyperfine Spin of a Cs Atom Ensemble, Phys. Rev. Lett. **99**, 163002 (2007).

[40] G. S. Agarwal, State reconstruction for a collection of two-level systems, Phys. Rev. A **57**, 671 (1998).

[41] P. Hyllus, O. Gühne, and A. Smerzi, Not all pure entangled states are useful for sub-shot-noise interferometry, Phys. Rev. A **82**, 012337 (2010).

[42] D. J. Wineland, J. J. Bollinger, W. M. Itano, F. L. Moore, and D. J. Heinzen, Spin squeezing and reduced quantum noise in spectroscopy, Phys. Rev. A **46**, R6797 (1992).

[43] S. A. Haine and S. S. Szigeti, Quantum metrology with mixed states: When recovering lost information is better than never losing it, Phys. Rev. A **92**, 032317 (2015).

[44] P. Ribeiro, J. Vidal, and Rémy Mosseri, Thermodynamical Limit of the Lipkin-Meshkov-Glick Model, Phys. Rev. Lett. **99**, 050402 (2007).

[45] T. Caneva, T. Calarco, and S. Montangero, Entanglement-storage units, New J. Phys. **14**, 093041 (2012).

[46] L. Pezzé and A. Smerzi, Ultrasensitive Two-Mode Interferometry with Single-Mode Number Squeezing, Phys. Rev. Lett. **110**, 163604 (2013).

[47] D. F. Walls and G. J. Milburn, *Quantum Optics*, 2nd ed. (Springer-Verlag, Berlin, 2008).

[48] S. A. Haine, Quantum noise in bright soliton matterwave interferometry, New J. Phys. **20**, 033009 (2018).

[49] In order to numerically evaluate the optimal value of the CFI in the presence of detection noise, we have considered the optimization of the measurement basis in the planes normal to $\hat{S}_n$ as well as $\hat{S}_x$.